NRC·CNRC

NRC Publications Archive
Archives des publications du CNRC

Electric field-tuneable crossing of hole Zeeman splitting and orbital gaps in compressively strained germanium semiconductor on silicon

Myronov, Maksym; Waldron, Philip; Barrios, Pedro; Bogan, Alex; Studenikin, Sergei

This publication could be one of several versions: author's original, accepted manuscript or the publisher's version. / La version de cette publication peut être l'une des suivantes : la version prépublication de l'auteur, la version acceptée du manuscrit ou la version de l'éditeur.
For the publisher's version, please access the DOI link below./ Pour consulter la version de l'éditeur, utilisez le lien DOI ci-dessous.

Publisher's version / Version de l'éditeur:
https://doi.org/10.1038/s43246-023-00431-x
Communications Materials, 4, 1, pp. 1-9, 2023-12-05

NRC Publications Archive Record / Notice des Archives des publications du CNRC :
https://nrc-publications.canada.ca/eng/view/object/?id=cd1dafbd-0ab3-4a10-ad53-9c90b5df2cf9
https://publications-cnrc.canada.ca/fra/voir/objet/?id=cd1dafbd-0ab3-4a10-ad53-9c90b5df2cf9

Access and use of this website and the material on it are subject to the Terms and Conditions set forth at
https://nrc-publications.canada.ca/eng/copyright
READ THESE TERMS AND CONDITIONS CAREFULLY BEFORE USING THIS WEBSITE.

L'accès à ce site Web et l'utilisation de son contenu sont assujettis aux conditions présentées dans le site
https://publications-cnrc.canada.ca/fra/droits
LISEZ CES CONDITIONS ATTENTIVEMENT AVANT D'UTILISER CE SITE WEB.

Questions? Contact the NRC Publications Archive team at
PublicationsArchive-ArchivesPublications@nrc-cnrc.gc.ca. If you wish to email the authors directly, please see the first page of the publication for their contact information.

Vous avez des questions? Nous pouvons vous aider. Pour communiquer directement avec un auteur, consultez la première page de la revue dans laquelle son article a été publié afin de trouver ses coordonnées. Si vous n'arrivez pas à les repérer, communiquez avec nous à PublicationsArchive-ArchivesPublications@nrc-cnrc.gc.ca.

National Research Council Canada
Conseil national de recherches Canada

communications
materials

ARTICLE

Check for updates

https://doi.org/10.1038/s43246-023-00431-x OPEN

Electric field-tuneable crossing of hole Zeeman splitting and orbital gaps in compressively strained germanium semiconductor on silicon

Maksym Myronov [1✉], Philip Waldron[2], Pedro Barrios[2], Alex Bogan[2] & Sergei Studenikin [2✉]

With the emergence of the quantum computing era, the spin physics of engineered semiconductor materials with large and tuneable effective $g^{\star}$-factor, which is a measure of the interaction between the magnetic field and the spin of the particle, has become of great interest because it offers new physics and engineering tools for spin's manipulation and its addressable control. Here we suggest a semi-empirical method to determine out of plane effective $g^{\star}$-factor in high mobility 2D hole heterostructures. We experimentally study the electric-field tuneablity of effective $g^{\star}$-factor of holes in a strained germanium quantum well heterostructure. As a result of the material's engineering, the $g^{\star}$-factor can be tuned in a large range from 13 to 24 that corresponds to the tuneable Zeeman spin splitting of heavy holes in the range from smaller, to equal, and to larger than the orbital Landau level quantization gap.

[1] Physics Department, The University of Warwick, Gibbet Hill Road, Coventry CV4 7AL, UK. [2] National Research Council of Canada, 1200 Montreal Rd., Ottawa, Ontario K1A 0R6, Canada. ✉email: M.Myronov@warwick.ac.uk; Sergei.Studenikin@nrc-cnrc.gc.ca

With the advent of quantum computing, there is a fast-growing interest in developing solid-state spin-based devices, which rely on the manipulation and control of the spin of electrons or holes in a solid-state system. One of the key factors in achieving this control is the effective g^*-factor, which is a measure of the interaction strength between the magnetic field and the spin of the particle. Materials with a large and tuneable effective g^*-factor offer new opportunities for the advanced spin manipulation protocols required for improved performance of addressable quantum gates and other spin-based devices. In addition to their potential applications in spin-based devices, such materials also have important implications for fundamental research in quantum and condensed matter physics. They may provide new insights into the spin interactions and spin-driven phase transitions in solid-state systems and offer new opportunities for exploring the quantum nature of matter.

A spin qubit in a semiconductor quantum dot is one the most promising platform for scalable quantum information processing devices, including quantum computers[1–3]. However, even for leading quantum computation platforms a large qubit circuit, consisting of 1 Million qubits, would require a huge area chip equal to a soccer field![4–6] In contrast to it, the same 1 Million qubits made of the compressively strained germanium on silicon (cs-GoS) material platform[7] would occupy an area smaller than 200 mm diameter epi wafer. Holes, the empty states in the valence energy band, have an internal angular momentum motion parameter called spin, which is a purely quantum mechanical property with no classical analog. Spin plays an important role in determining the behavior of particles in a magnetic field and their interactions with other particles. Spin can be imagined as an internal inherent spinning or rotation of the elementary charge around the axis, schematically shown in Fig. 1a. Particles with spin $s = 1/2$, such as electrons, are ideal microscopic objects for spin qubits. Holes in the valence band have a total angular momentum of $J = 3/2$, but they still can serve as an excellent basis for qubits with enhanced capabilities if the light hole (LH) band states $J_z = \pm\frac{1}{2}$ are split from the heavy hole (HH) band $J_z = \pm\frac{3}{2}$ by strain, the spin-orbit interaction and/or the vertical z-quantization in a quantum well (QW).

Figure 1b shows an energy level schematic of a QW filled with free carriers at zero temperature and in zero magnetic field, B, (left diagram) and for $B > 0$ (right diagram). In zero B-field, free Fermionic carriers occupy states of the conduction or valence band up to the Fermi energy, E_F. In non-zero field the 2D free carriers' spectrum is further quantized into the discrete, degenerate Landau levels (LL), each of which is split by the Zeeman, E_Z, energy into two spin sublevels. Even or odd number, ν, called the filling factor of the discrete levels, can be occupied, depending on the magnetic field strength and the 2D carrier areal density.

The effective g^*-factor is the key parameter of spin qubits characterizing the Larmor precession frequency or, equivalently, the energy separation between the spin-split Zeeman energy levels, given by $E_Z = g^*\mu_B B$, where μ_B is the Bohr magneton, and B is the magnetic field.

The topic of electrically tuneable effective g^*-factor has attracted broad interest from both scientific and quantum device engineering perspectives over the last two decades. With the emergence of worldwide interest in the field of quantum computing, the effective g^*-factor has attracted even broader attention as a critical characteristic of spin qubits for engineering large and scalable quantum circuits with the capability of addressing individual qubits required for quantum algorithms and the storage and readout of quantum information[3,8–13].

Many mechanisms for tuning the g^*-factor have been reported in the literature, but modifying the g^*-factor of conduction band (CB) electrons has proven to be challenging because it requires barrier materials having a different material's g^*-factor and small CB non-parabolicity[14,15] or uses a compositionally graded parabolic QW[16]. To tackle these issues tuneable micromagnet technology was introduced[17] that relied on the B-field gradients (δB_i) created by small, micro-sized magnets. Being helpful and widely adopted[18–21] this technology has strong limitations due to very close distances between neighboring qubits required to produce necessary δB_i gradients at the individual sites, i.

Particularly in silicon (Si) devices, the effective g^*-factor of an electron bound to a donor can also be tuned by applying an external electric field, which is known as the Stark effect[8,22]. This effect arises from the interaction between the electric field and the

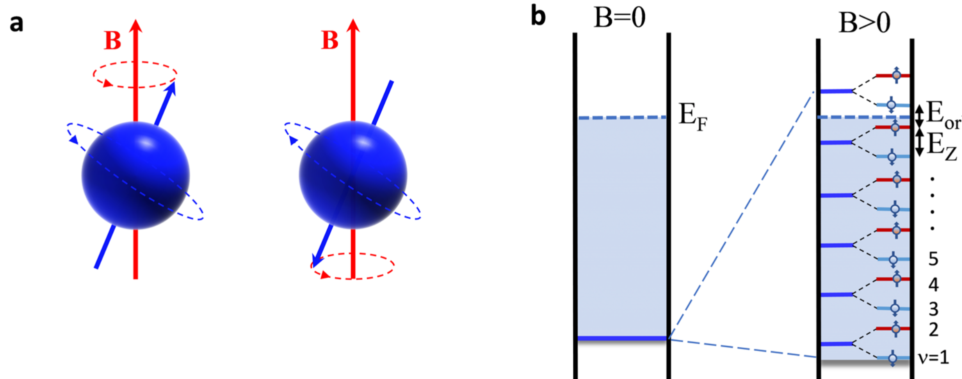

Fig. 1 A schematic visualization of effective spin 1/2 hole or electron quasiparticles and their Fermi-distribution in a quantum well with and without external magnetic field. a A visualization of an elementary charge particle with internal quantum motion leading to quantized internal orbital momentum in Plank's constant $\hbar$ and associated magnetic momentum characterized by the effective g*-factor, $g^*\mu_B$, where $\mu_B = e\hbar/2m_e$ being the Bohr magneton; Electrons have 1/2 spin which can be either up or down. When a magnetic field is applied to a magnetic moment, then the moment experiences a torque to try to align the moment with the field to minimize energy. **b** Energy schematic of the quantum well filled with free carriers at zero temperature in zero magnetic field (B = 0, left image) and for B > 0 (right image). In zero field (B = 0) free Fermionic carriers occupy states of the band up to the Fermi energy, E_F. In non-zero field the free carriers' spectrum is quantized in discrete degenerate Landau levels (LL), each of them is split by the Zeeman energy, E_Z, in two spin sublevels. The two-dimensional hole gas (2DHG) energy spectrum is characterized by the Zeeman and orbital gaps, E_Z and E_{orb}, respectively. Even or odd number of the discrete levels is occupied, called the filling factor, ν, depending on the magnetic field strength and the 2D carrier areal density controlled by the gate voltage in a field-effect device.

orbital motion of an electron bound to an impurity, which can shift the electron's energy levels and change its effective g^*-factor. The Stark effect has been used to tune the effective g^*-factor of electrons in Si-based spin qubits, but this mechanism permits changes of the effective g^*-factor, $\delta g^*(V)$ that is too small to be practical in large scale circuits. The demonstrated frequency tuning range is limited to ~1 MHz/V at $B_0 = 1.55\,T$ or a corresponding resonance frequency ~43 GHz[8] that is equivalent to a g^*-factor change of just 0.002%.

An electrical tuneability of effective hole g^*-factor in Si quantum dots (QDs) was studied in refs. [23,24], where a much larger range of g^*-factor tuneability compared to the g^*-factor Stark shift[22] was shown. In particular, in ref. [23] a strong anisotropy of g^*-factor was observed in a Si planar metal-oxide-semiconductor quantum dot [see Supplementary Note 3 for more details] and its variation by a local gate in the range about from 1.2 to 2.5. The effective g^*-factor tuning with local gates is a very useful functionality for small-scale qubit devices, but may cause certain challenges for large-scale applications, e.g., beyond a thousand qubits in which every qubit has to be carefully tuned and calibrated. Therefore, it is desirable to create materials with tuneable g^*-factor defined by the material's stack. In other words, search for materials with large g^*-factor tuneability is desired for spin applications. Let us emphasize once more, one should distinguish between a QD device-level and the material's g^*-factor tuneability. In the first case, effective g^*-factor is controlled by local gates of a specific QD device in 3D geometry space. In the second case, g^*-factor is tuned by a global gate in 1D, producing normal, i.e., vertical electric filed along the growth direction. Therefore, the material's g^*-factor engineering is more appealing from the practical point of view for large scale devices when it is preferable to have predictable and identical qubits defined purely by the material's stack properties.

The development of high-quality *p*-type semiconductor materials and successful single-hole spin devices demonstration has led to various novel opportunities for g^*-factor research and engineering. The more complex energy band structure of the valence band, involving LH and HH bands combined with their strong spin-orbit interaction holes offer unique opportunities for tuneable g^*-factor engineering required for practical realizations of large qubit arrays[1–3,25]. There are many more mechanisms for tuning of the g^*-factor in QD devices by employing discrete energy spectra of QDs. One of a such g^*-factor's tuning mechanisms was reported in a lateral p-GaAs double quantum dot operating in a single-hole regime employing spin orbit interaction (SOI) with an empty level of an auxiliary QD[13,26]. For electron devices this mechanism does not work because the CB SOI is too weak. For the valence band holes, most of works mentioned above were devoted to different mechanisms of the g^*-factor tunability utilizing QD gated devices. However, the essential and very desirable mechanism would be the one that would allow an ultimate g^*-factor control in an engineered material, e.g., using a classical field effect transistor (FET)-like operation by an electric field perpendicular to the surface. The quantum properties of such devices could be more reliably designed and engineered because they rely on the 2D hole band structure defined by the material's stack, which can be simulated theoretically and carefully controlled by epitaxial growth techniques. This would essentially reduce complexity of the expensive calibration processes of large qubit circuits[27].

Small carrier effective mass m^* is another very valuable property for quantum qubit architectures. A small effective mass allows for relatively large dimensions of the QD's lateral confining potential formed by the surface split gates[28]. The 3D shape of the resultant QD confining potentials becomes very flat, with the lateral in-plane dimensions being much larger than the vertical confining QW thickness. Therefore, the QDs attain a very pronounced 2D character defined by the material's stack. In addition, larger lateral size of QDs leads to suppression of nuclear effects due to averaging over a larger number of nuclei[29]. And the last, but a very important feature offered by small m^* is larger lateral QD dimensions, which allows positioning QD spin qubits deeper below the surface that is vital for reduction of all sorts of noise effects produced by unavoidable surface charges and defects[3].

Holes in compressively strained germanium (s-Ge) possess unique properties compared to other semiconductors, including p-Si and p-GaAs. Recently, it has been shown that holes in s-Ge QW heterostructures outperform electrons in all group-IV semiconductor materials by a number of metrics[7], including greater free carrier hole mobility ($>4 \times 10^6\,\mathrm{cm^2V^{-1}\,s^{-1}}$), lower percolation density and effective mass, which can be engineered to be as small as $0.035\mathrm{m_0}$. Moreover, Ge has a centrosymmetric crystal structure and therefore does not inherit the large bulk Dresselhaus component of SOI that would arise from bulk inversion asymmetry[7]. The bulk Dresselhaus SOI is very strong in III–V compound semiconductors, which causes additional spin-orbit (SO) mediated decoherence processes that are harmful for spin qubit devices[30]. On the other hand, SO is a useful interaction mechanism if it can be controlled, which is exactly the case for s-Ge devices that have structural inversion asymmetry in the growth direction. Indeed, in s-Ge structures only the Rashba SO component remains active, which can be engineered and controlled by a gate voltage of a FET device. This allows for rapid on-off switching, which is desirable for spin manipulations and quantum information processing[2,31]. The Rashba-type SOI is advantageous compared to Dresselhaus coupling[32], whose coupling parameter is a bulk material constant that cannot be tuned by external electric fields.

In this article we suggest a semi-empirical method to determine out of plane effective g^*-factor in high mobility 2D hole s-Ge QW heterostructures. We experimentally study the electric-field tuneablity of effective g^*-factor of holes in large gated Hall bar devices, fabricated from a s-Ge QW heterostructures, epitaxially grown on a standard Si wafer, whose spin properties are fully defined by the material's stack. As a result of the material's engineering, the g^*-factor can be tuned in a large range from 13 to 24 that corresponds to the tuneable Zeeman spin splitting of heavy holes in the range from smaller, to equal, and to larger than the orbital Landau level quantization gap. The obtained results are appealing to studies of fundamental physics, e.g., the ferromagnetic phase transitions and the fractional quantum Hall effect involving spin states, and also open new opportunities for developments of spin-based devices such as qubits, spin field-effect and spin-orbit transistors, including their operation at elevated temperatures at and above ~4 K.

Results and discussion

Here we report on the new method of extraction of the semiconductor material's effective hole g^*-factor, tuneable by the external electric field and realized in a s-Ge QW heterostructure FET-like Hall-bar device. The cross-section of the gated Hall-bar device along with a 3D drawing are shown in Fig. 2a, b, respectively. A two-dimensional hole gas (2DHG) is created in a 15 nm thick s-Ge QW positioned ~100 nm below the semiconductor/dielectric interface and controlled by applying a negative gate voltage. The current flows between the source and drain contacts of the Hall-bar device. The longitudinal magnetoresistivity, $\rho_{xx}(B)$, and the Hall-effect resistance, $R_{xy}(B)$, are measured using the corresponding potential probes along and across the Hall bar.

Figure 2c–e show three selected traces of magnetoresistivity and the filling factor calculated from measured Hall resistance,

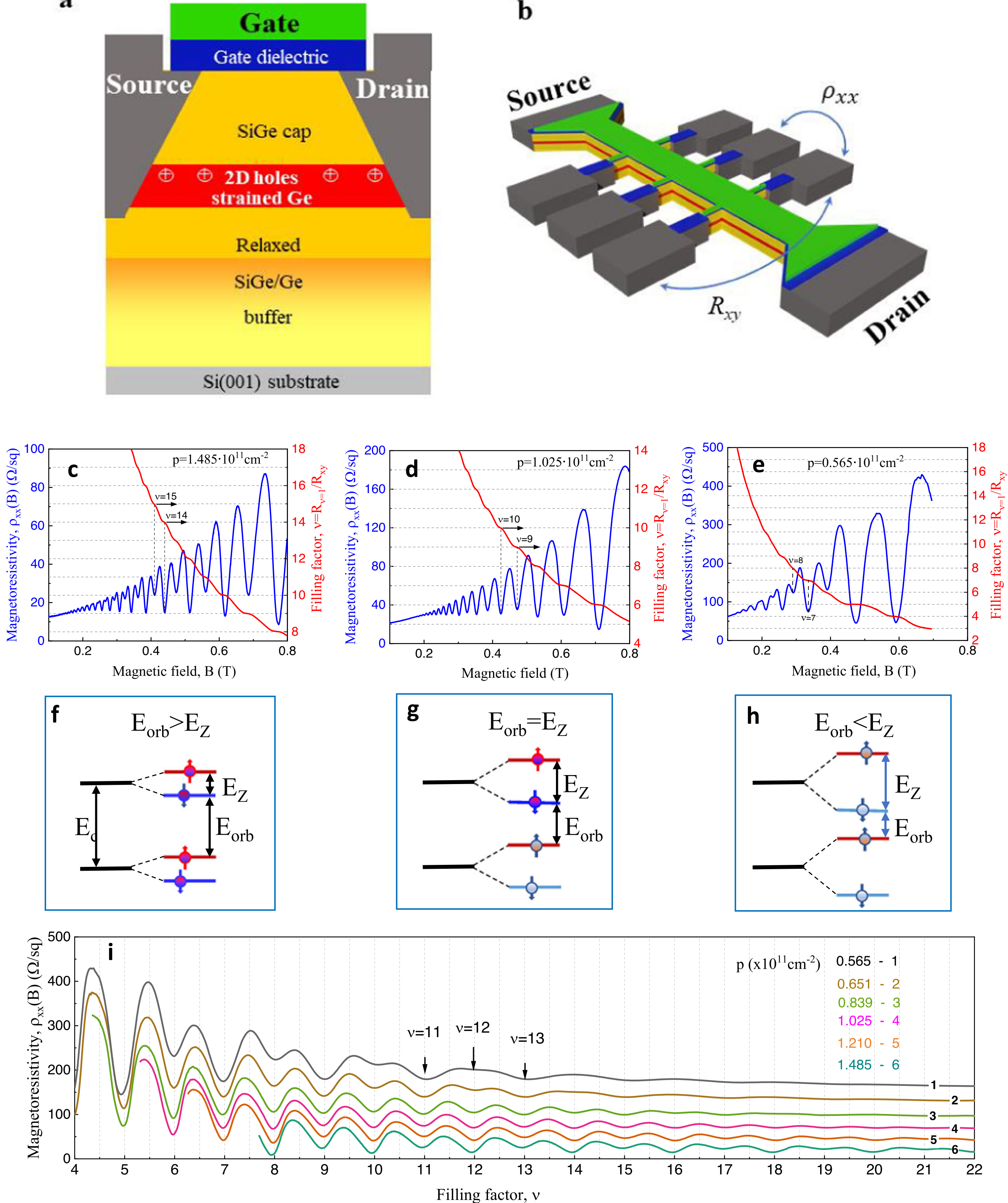

Fig. 2 Device schematic and Shubnikov-de Haas (SdH) traces for the three special situations. **a** Cross-section schematic of the material's stack in the fabricated devices; a 15 nm s-Ge QW is positioned ~100 nm below the dielectric /semiconductor interface. The magnetic field is applied normal to the surface (for more details see text). **b** 3D-visualization of the gated Hall bar device. **c**, **d**, **e** The magnetoresistivity, $\rho_{xx}(B)$, and corresponding filling factor traces $\nu = R_1/R_{xy}$, for three selected values of hole densities. **f**, **g**, **h** diagrams of the level structure for the traces shown above, E_{orb} being orbital and E_Z being the Zeeman splitting gaps. **i** Magnetoresistivity traces as a function of the filling factor for selected hole densities, p, in the range of $0.565–1.485 \times 10^{11}\ \mathrm{cm}^{-2}$.

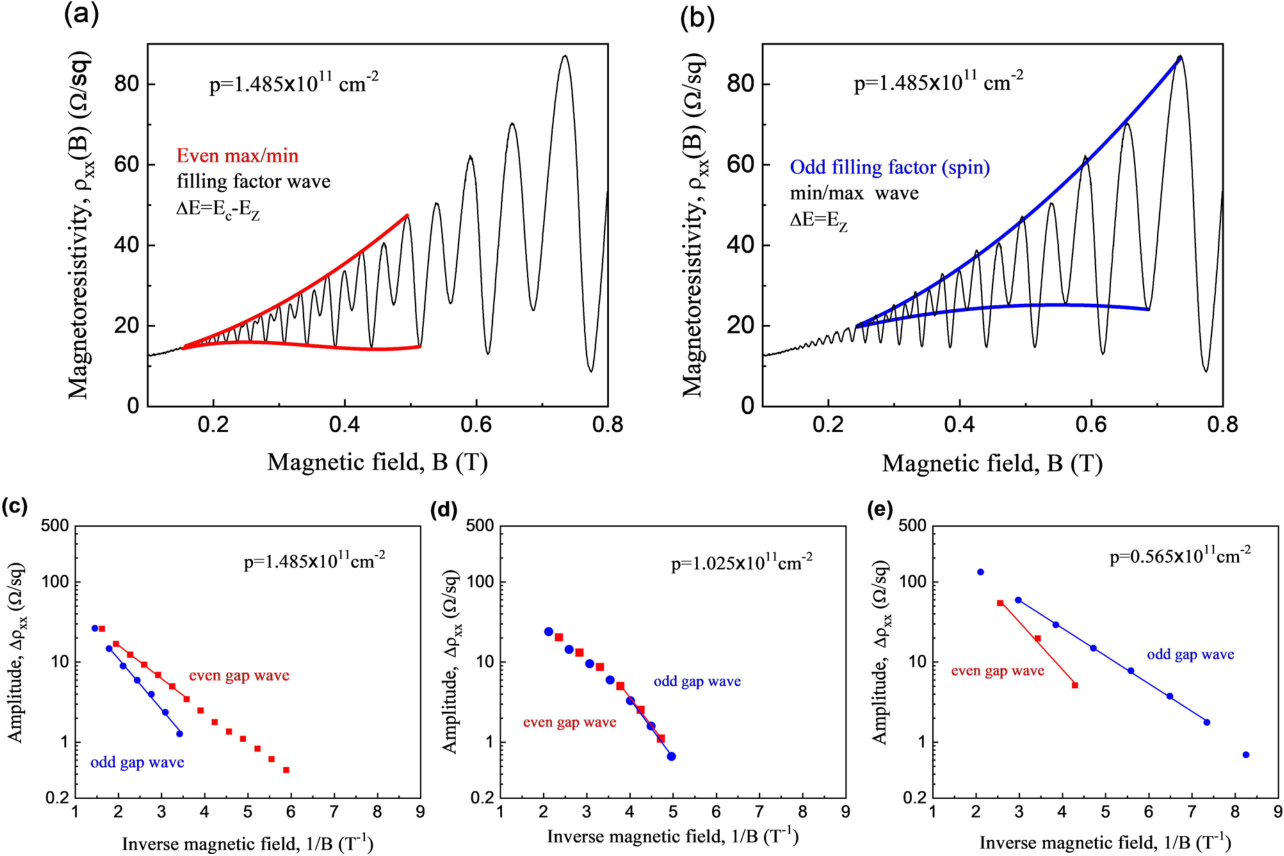

Fig. 3 An example of the SdH traces with even (orbital) and odd (spin) waves highlighted along with the Arrhenius plots of the SdH amplitude. **a**, **b** The magnetoresistivity trace at $p = 1.485 \times 10^{11} cm^{-2}$ containing two-component SdH oscillations defined by orbital or Zeeman gaps corresponding to the even or odd filling factors. For clarity, the orbital/Zeeman components are marked by the thick envelope lines in (**a**) and (**b**) correspondingly. **c**, **d**, **e** Examples of the Arrhenius-type analysis of the orbital (even) and Zeeman (odd) wave components for the three selected concentrations (marked in the graphs) corresponding to traces in Fig. 2c–e.

R_{xy}, as $\nu = R_1/R_{xy}$ (left and right scales correspondingly), where $R_1 = \frac{h}{e^2} = 25812.80745\,\Omega$ is the von Klitzing constant and h is Planck's constant[33]. Figure 2f–h show the energy levels schematics corresponding to the three traces above them. Figure 2i shows selected magnetoresistivity traces as a function of the filling factor, $\nu = p\hbar/Be$, which in turn varies with inverse magnetic field. The magnetoresistivity minima and the Hall effect plateaus occur at odd and even integer filling factors ($\nu = 11, 12, 13$ are marked by arrows in Fig. 2i).

A careful analysis of the Shubnikov-de Haas (SdH) oscillations and the R_{xy} quantization levels of the Hall conductance, $\nu = R_1/R_{xy}$, (right axis of Fig. 2c–e) allows us to identify the hierarchy of the energy gaps as a function of carrier density. Qualitatively, the depth of the minima associated with odd/even values of ν decay exponentially with the size of the energy gaps associated with the orbital (E_{orb})/Zeeman (E_Z) splitting. It is evident in Fig. 3c that the minima associated with even filling factors are deeper those of the odd minima (e.g., compare $\nu = 14$ and 15 indicated in the graph). This implies that the orbital gap between LLs (E_{orb}) is larger than the Zeeman spin gap (E_Z). This ordinary situation, shown in Fig. 2f, occurs in most semiconducting materials including narrow band gap semiconductors like InSb, where the electron g*-factor is ~50[34]. In contrast, Fig. 2e shows the reverse situation: minima associated with odd ν are deeper than those of even ν, indicating $E_{orb} < E_Z$.

However, Fig. 2d, shows the crossover regime, where the minima of even and odd filling factors are equal for the whole range of magnetic field and the SdH oscillations disappear completely at small fields. The same cross-over value is confirmed in an additional experiment on another device, made from the same epiwafer, but presented in the Supplementary Note 1. This situation corresponds to the condition of the equally spaced energy level ladder shown in Fig. 2g, where the spin and orbital quantization gaps are equal, $E_{orb} = E_Z$. This, so-called coincidence method was employed to determine g^*-factor of electrons using tilted magnetic fields to regulate the ratio E_Z/E_{orb}[35]. It should be stressed that the tilted field technique does not generally work for holes due to the very strong g*-factor anisotropy, with its in-plane component close to zero[30]. But the s-Ge QW material provides unique opportunity to tune g^*-factor, by the accumulation gate voltage tuning, in a large range, including crossing at the coincidence point. This allows us to reliably determine the hole g^*-factor at this specific condition; the analysis will be discussed later.

From the next panel of Fig. 2e it is evident that the situation has reversed compared to the panel of Fig. 2c: the odd (spin) minima are deeper than the even (orbital) minima. It qualitatively proves that in this condition the Zeeman gaps are larger than the orbital ones, as sketched in the corresponding level diagram in Fig. 2h. The same conclusion can be deduced from the evolution of odd/even peaks (e.g., $\nu = 11, 12, 13$) presented in Fig. 2i.

To summarize, Fig. 2 qualitatively demonstrates that in a s-Ge QW heterostructure the effective hole g^*-factor can be efficiently tuned by the accumulation gate voltage (FET-like operation), making it capable of reaching all three important regimes: where the Zeeman splitting is smaller ($E_Z < E_{orb}$), equal ($E_Z = E_{orb}$) and

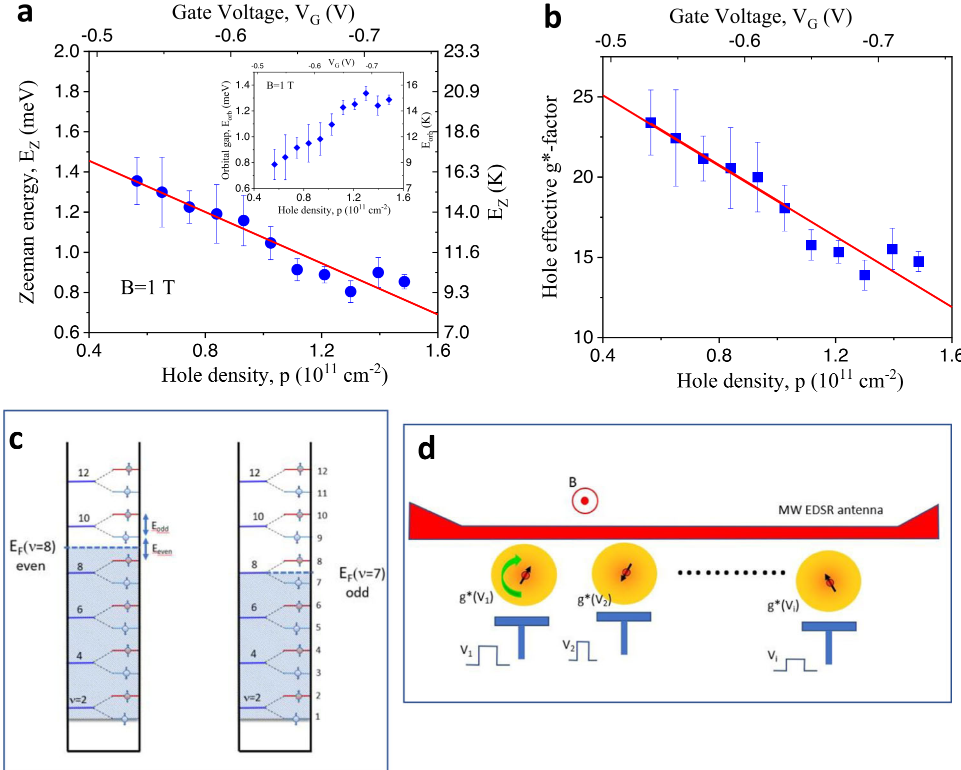

Fig. 4 Spin-split Zeeman energy as a function of the gate voltage controlling perpendicular electric filed and hole density, along with the qualitative visualization of spin-split hole levels in a magnetic field and proposed scalable spin-qubit architecture. a Zeeman spin split energy at B = 1T as a function of hole density controlled by the gate voltage (plotted as top axis) determined from the Arrhenius analysis shown in Fig. 3c–e. The right scale is given in temperature units. Insert shows the orbital splitting of the Landau levels ladder shown in (**c**). **b** Hole effective g^*-factor as a function of density (gate voltage), line is the fit function $f = 29.5–11.0$ p; error bars in (**a**) and (**b**) are defined as one standard error deviation determined in the fitting procedure of Arrhenius plots. **c** schematic of the Landau levels filled by degenerate 2D hole gas for two situations, when Fermi level position is located in the orbital gap (left) or between the spin split levels (right) corresponding to even and odd series of SdH oscillations. **d** A sample schematic for a scalable spin-qubit architecture using the gate-tuneable g^*-factor.

larger $E_Z > E_{orb}$ than the orbital ($E_{orb} = E_c - E_Z$) quantization gap. Details of the spin and orbital gaps analysis, which was used to determine the effective g^*-factor can be found in the Methods section of the article.

Figure 3a, b show an example of the SdH oscillations for the 2DHG carrier density of $p = 1.485\times 10^{11}\mathrm{cm}^{-2}$. Two components of SdH oscillations are evident, which correspond to even (orbital) and odd (spin) filling factors. For clarity, these even and odd components, termed waves, are marked with thick lines in panels (a) and (b), respectively. A schematic energy spectrum corresponding to the odd and even waves of the SdH oscillations is presented in Fig. 4c. Uniquely, our devices provide odd and even waves that have a sufficient number of oscillations for the Arrhenius-kind analysis in the small-field region where the oscillation amplitude is sensitive to the E_{orb} and E_Z energy splitting, shown in Fig. 3c–e. Following standard SdH equations[36,37] we assume that the amplitude of exponentially decaying even/odd SdH waves is described by $A_{even} \propto \exp(-\frac{\pi\hbar}{\mathrm{E_{orb}}\tau_q})$ and $A_{odd} \propto \exp(-\frac{\pi\hbar}{\mathrm{E_Z}\tau_q})$, where τ_q is the quantum relaxation time, $\mathrm{E_{orb}} = E_c - E_Z = (\frac{\hbar e}{m^*} - g^*\mu_B)B$, where $\mu_B = \frac{e\hbar}{2m_0}$ is the Bohr magneton, and m_0 is the free electron mass. In our semi-empirical approach to determine the effective g^*-factor we use the ratio of two slopes $\alpha = k_{orb}/k_Z$ with k_Z and k_{orb} corresponding to the fit slopes in the semi-logarithmic scale vs 1/B of odd and even waves in Fig. 3c–e. The advantage of this method is that the odd/even SdH waves occur in the same B-range and therefore does not require any assumption about possible B-dependence of the $\tau_q(B)$ that is still a challenging problem to identify experimentally[38]. From the above equation, we can write $\alpha = (E_c - E_Z)/E_Z = E_c/E_Z - 1$ and find the effective g*-factor from the experimentally determined ratio of even/odd slopes α: $g^* = \frac{\hbar e}{\mu_B m^*}\frac{1}{\alpha+1} = \frac{2}{\alpha+1}\frac{m_0}{m^*}$.

The hole effective mass $m^* = 0.054m_0$ is determined from the temperature dependence of the amplitude of SdH oscillations in small magnetic fields in the high-density regime where cyclotron LL oscillations dominate, i.e., when the spin splitting is not resolved[37,39]. There may be some variation of the effective mass with the hole density due to hole–hole interaction[37,40], and/or due to variations of the valance band energy spectrum caused by the strong vertical electric filed[41]. We argue that a possible small change of m^* would be much smaller than the overall tuneable variation of the effective g^*-factor reported here [see Supplementary Note 2 for details]. Figure 3c–e show Arrhenius analysis plots of the odd/even waves of the SdH amplitude versus the inverse magnetic field corresponding to the SdH traces of Fig. 2c–e. We emphasize that the spin (odd) and orbital (even) SdH waves occur in the same magnetic field range; no assumptions are therefore required about the possible field dependence of the LL width[12,38,42].

The results of the outlined analysis are presented in Fig. 4. The Zeeman spin split energy is plotted in Fig. 4a for magnetic field of $B = 1$ T, and the effective g^*-factor is plotted in Fig. 4b. It is evident from Fig. 4a that the spin splitting can reach values of over 1.35 meV, or equivalently ~16 K (right axis), which bodes well for the possibility of spin devices operating at temperatures

above 10 K. This is an important milestone in the development of new materials for high temperature qubit operation as a larger Zeeman spin splitting is desirable for higher fidelity operations and readout[3,43–45]. Nowadays, single spin qubit operation in Si devices at higher temperatures is indeed limited by the Zeeman energy[43,44] as the qubit efficiency reported in references[43,44] quickly deteriorates for temperatures above 1 K. The obtained hole effective g^*-factor, shown in Fig. 4b, increases from ~13 up to 24 as the 2DHG density decreases from ~1.5×10^{11} cm^{-2} down to ~0.5×10^{11} cm^{-2}, respectively. In contrast to published theoretical predictions[46], the effective g^*-factor measured in this s-Ge material could in principle reach values as large as $g* \approx 29$ for smaller 2DHG densities, assuming linear extrapolation of the obtained results in Fig. 4b and also reported in[47].

As discussed in refs. [28,46], hole's g^*-factor is very sensitive to relative position of heavy and light hole states. In general, the valance band levels can be described by a reduced 4×4 Luttinger-Kohn Hamiltonian[46], or by full 6×6 Luttinger-Kohn-Bir-Pikus (LKBP) Hamiltonian[28]. Compared to CB electrons, which g^*-factor has very small variations due to external fields[14,15], hole's effective g^*-factor strongly depends on specific parameters of the material's stack and on details of interaction and mixing LH and HH states confined in the quantum well structure[28,46].

The g^*-factor tuneability by a local gate is a very valuable feature for designing scalable quantum computing architectures based on the solid-state spin qubits. One example of such a scalable qubit architecture is shown in Fig. 4d. A global, continuous microwave (MW) excitation field can be provided, for example, by a MW strip-line antenna, as depicted schematically in the diagram[8,48] or, i.e., by using a three-dimensional dielectric resonator[49]. Selected qubits can be tuned in the Electric Dipole Resonance (EDSR) condition by pulsed gate voltages using $g^*\left(V_i\right)$ to make required quantum-gate operations, while other qubits stay off-resonance for storing quantum information or awaiting future processing. In our proposed device architecture there is no need for pulsed magnetic fields or micromagnet technology. Operation with DC gate pulsing is sufficient, which simplifies the design of scalable qubit circuits significantly[3]. Therefore, the demonstrated large and tuneable hole's g^*-factor in the s-Ge semiconductor material offers the unprecedented potential for spin-qubits that would operate at desired elevated temperatures equal or above 4 K. This compares favorably to hole-based spin devices in Si, with $g^*(\mathrm{Si}) \approx 2$ implying operating temperatures around 1 K in a magnetic field of 1.6 T[43].

Methods

Epitaxial growth of s-Ge QW heterostructures. For the reported research, undoped s-Ge QW heterostructures were grown by RP-CVD on a relaxed $Si_{0.15}Ge_{0.85}$ buffer on a standard Si(001) wafer of 150 mm diameter[7,39,50]. A schematic cross section of the heterostructure and fabricated gated Hall bar device, with its source (S) and drain (D) ohmic contacts and gate (G) stack is shown in Fig. 2a. All epilayers were intentionally undoped. Accumulated by the negative gate voltage, holes are confined in the 15 nm thick undoped QW, positioned ~100 nm below the $Si_{0.15}Ge_{0.85}$ spacer and ~1 nm thick Ge cap interface. A thick $Si_{0.15}Ge_{0.85}$ spacer epilayer was intentionally selected to minimize impact of the remote ionized impurities located at the Ge cap/Al_2O_3 gate dielectric interface and within the gate dielectric[50].

Field effect gated Hall bar devices microfabrication. For magnetotransport characterization of 2DHG vs. gate voltage, gated Hall bars were fabricated using standard UV lithography, dry etching and thin film deposition techniques[7]. Fig. 2b shows a 3D image of a Hall bar with its channel oriented along the <110> in-plane crystallographic direction[39] and defined by the mesa structure etched in a Cl_2/Ar plasma. The Hall bar's channel width is 100 µm and the distance between adjacent contacts is 200 µm. The alloyed AlSiGe Ohmic contacts were prepared by evaporating a 120 nm thick Al film and annealing at ~275 °C in N_2 ambient for 30 min. The contacts show low resistivity and excellent linear ohmic behavior at cryogenic temperatures. The top accumulation gate is made of 20 nm Ti followed by 200 nm Au on a 50 nm thick Al_2O_3 dielectric layer deposited by Atomic Layer Deposition at 200 °C.

Magnetotransport characterization. The gated Hall bar was mounted in a ^{3}He cryostat equipped with a superconducting solenoid. For the low-temperature transport measurements, we employed a standard lock-in technique with an excitation current, I, of 20 nA limited by a 1 MΩ in-series resistor. We used two synchronized lock-in amplifiers at 88 Hz to measure longitudinal (U_{xx}) and transverse or Hall (U_{xy}) voltages simultaneously. Zero magnetic field resistivity, $\rho_{xx}(0) = wU_{xx}/IL$, and the Hall voltage in a small magnetic field were measured to calculate carrier density $p = \frac{B}{eR_{xy}}$ of 2DHG and carrier transport mobility, $\mu = \frac{R_{xy}(B)}{B\rho_{xx}(0)}$. A gate voltage applied between the gate G and the drain D was used to change the electric field across the QW structure and control the 2DHG density accumulated in the s-Ge QW channel.

SdH oscillations analysis to obtain g*-factor. The SdH oscillations of magnetoresistivity is an equilibrium transport phenomenon determined by the free carriers' diffusive motion at the Fermi level within the thermal broadening of the Fermi distribution function. Thanks to the small hole effective mass and large g^*-factor, in our experiment the temperature correction factor is small, less than 10% at $B \geq 0.3T$, where the Arrhenius analysis is performed (Fig. 2c–e). We therefore ignore the temperature correction and defer consideration to future work. We use the ratio method (discussed below) of the slopes measured in the same range of magnetic fields, which compensates for possible uncertainties due to unseen corrections due to temperature or unknown shape of the LL function. For previous methods used to determine effective g^*-factor from SdH oscillations see Supplementary Note 4.

In two dimensions the free carrier systems the density of states (DOS) is a constant function: $\mathrm{DOS} = \frac{m^*}{\pi\hbar^2}$. All available states below the Fermi level are filled, while above they are empty as is schematically shown in Fig. 1b (left diagram). In a magnetic field the free carrier DOS becomes discrete and is described by the LL's energy spectrum $E_{LL} = \left(\frac{1}{2} + N\right)\hbar\omega_c \pm \frac{1}{2}g^*\mu_B B$ and a corresponding DOS[38,51,52], where N is the LL orbital quantization number. It is a very challenging problem to determine the precise shape of the DOS, both theoretically[53] and experimentally[54]. SdH oscillations arise due to the LL ladder moving relative to the Fermi level as the magnetic field changes. In principle, SdH oscillations cannot be used for spectroscopy of a strongly quantized energy spectrum of free carriers because the Fermi level is not constant and quickly jumps between the LL levels[55]. However, in relatively small magnetic fields where LL are not fully separated, the SdH amplitude, A_{SdH}, becomes sensitive to the energy separation between the levels. We exploit this spectroscopic regime here to probe E_{orb} and E_Z.

In the spectroscopic regime A_{SdH} depends on the shape and width of the LL DOS[38,51,52]. In the case where spin splitting is not resolved and the orbital splitting is defined by the cyclotron energy $\hbar\omega_c = \frac{\hbar eB}{m^*}$, the SdH amplitude decays exponentially with

the inverse magnetic field: $\frac{\Delta\rho_{xx}}{\rho_0} = 4\exp\left(-\frac{\pi}{\tau_q\omega_c}\right)D_{th}(X_T)$, where τ_q is the quantum relaxation time and $D_{th} = X_T/\sinh(X_T)$ is the thermal damping factor with $X_T = 2\pi^2 k_B T/\hbar\omega_c$[36,37] While this equation assumes the LL DOS is either Lorentzian with constant width, Γ_L, or Gaussian with $\Gamma_G \propto \sqrt{B}$[38,52], it is often used to determine the effective mass from temperature damping measurements[37] even when the shape of the LL DOS is not known. Applying this approach in the high-concentration range where Zeeman splitting is not resolved in the small field range, i.e., where the LL separation is determined by the cyclotron energy $\hbar\omega_c$, we determine $m^* = 0.054m_0$.

Due to the electron–electron (e–e) exchange interaction, the resultant spin-splitting is a complex problem requiring the self-consistent Born approximation (SCBA) approach to determine the B-dependent broadening of LLs, and the exchange contribution to the spin splitting energy[37,53,56,57]. Experimentally the e–e interaction leads to a very strong effective g^*-factor enhancement; in materials with small bare g^*-factor such as GaAs, we have $g^*(\text{GaAs}) \approx 0.44$[38,58,59]. The exchange contribution to the g^*-factor depends on the filling factor, temperature, and LL broadening, and is further complicated by the important role of the LL shape in the SCBA approach. This challenging issue is still not fully resolved and requires further experimental studies and theoretical attention. Here we have developed a semi-empirical approach to tackle the above problem in order to gain reliable information about the material's g^*-factor and its tunability. Several features of the presented s-Ge material system allow us to gain this information. First, the effective g^*-factor in the presented material is very large compared to CB electrons in GaAs ($g^*(\text{GaAs}) \approx 0.44$) and Si ($g^*(\text{Si}) \approx 2$). In addition, the hole effective g^*-factor is tuneable in large range that allows us to reach the three special conditions shown in Fig. 2c–e that is important to reliably determine g^*-factor, in particular, at the coincidence point shown in Fig. 2d.

As a consequence of the very large carrier mobility of more than 4×10^6 cm^2V^{-1} s^{-1} [7], we are able to observe a large number of SdH oscillations down to very small fields (B ~ 120 mT). The SdH oscillations, e.g., displayed in Fig. 2c–e, and Fig. 3a, b clearly reveal two distinct, well resolved components corresponding to even and odd filling factors (herein referred to as *odd* and *even* waves). These two components appear in the same range of small magnetic fields when the SdH minima do not reach zero and therefore are sensitive to the LL broadening and the energy gaps, E_{orb} and E_Z. These factors allow us to develop a semi-empirical method (described in the main text) to attain information about the effective g^*-factor.

Note, that g^*-factor in the reported s-Ge material is over 10 times larger than that of other materials, including group-IV and III–V semiconductors. Additionally, in our gated Hall bar devices, metallic gate is positioned at a distance of 150 nm from the 2DHG (a 100 nm SiGe cap epilayer plus a 50 nm Al_2O_3 gate dielectric). This is comparable to the average distance between carriers, $\langle r \rangle$, which is ≈ 30 nm for $n_s = 10^{11}$ cm^{-2}. Under these conditions, the metallic gate produces essential screening of the Coulomb e–e interaction and therefore reduces the correction to the effective g^*-factor enhancement due to the e–e exchange interaction[55,57]. Other mechanisms may lead to further suppression of the g^*-factor exchange contribution in hole systems due to HH-LH interaction[60]. More rigorous theoretical analysis is required to carefully investigate the remaining exchange interaction effects in FET-like gated hole devices like one under the discussion here. Based on the above, we argue that exchange contribution is small compared to the bare material g^*-factor and we can therefore neglect it here in order to extract information about the material effective g^*-factor and its tunability with the gate voltage in a FET-like gated structure using the Arrhenius-kind analysis, described in the main text.

Data availability

All data are available in the main text and supplementary materials. Any additional data are available from the corresponding author upon request.

Received: 25 October 2023; Accepted: 16 November 2023;
Published online: 05 December 2023

References

1. Stano, P. & Loss, D. Review of performance metrics of spin qubits in gated semiconducting nanostructures. *Nat. Rev. Phys.* **4**, 672–688 (2022).
2. Scappucci, G. et al. The germanium quantum information route. *Nat. Rev. Mater.* **6**, 926–943 (2021).
3. Burkard, G., Ladd, T. D., Pan, A., Nichol, J. M. & Petta, J. R. Semiconductor spin qubits. *Rev. Mod. Phys.* **95**, 025003 (2023).
4. *Charting the course to 100,000 qubits*, <https://research.ibm.com/blog/100k-qubit-supercomputer> (2023).
5. Gibney, E. Physicists propose football-pitch-sized quantum computer. *Nature* **542**, 151–151 (2017).
6. Storz, S. et al. Loophole-free Bell inequality violation with superconducting circuits. *Nature* **617**, 265–270 (2023).
7. Myronov, M. et al. Holes outperform electrons in Group IV semiconductor materials. *Small Sci.* **3** (2023). https://doi.org/10.1002/smsc.202200094
8. Laucht, A. et al. Electrically controlling single-spin qubits in a continuous microwave field. *Sci. Adv.* **1**, e1500022 (2015).
9. Prechtel, J. H. et al. Electrically tunable hole g factor of an optically active quantum dot for fast spin rotations. *Phys. Rev. B* **91**, 165304 (2015).
10. Voisin, B. et al. Electrical control of g-Factor in a few-hole Silicon Nanowire MOSFET. *Nano Lett.* **16**, 88–92 (2016).
11. Shchepetilnikov, A. V. et al. Spin-orbit coupling effects in the quantum Hall regime probed by electron spin resonance. *Phys. Rev. B* **98**, 241302 (2018).
12. Sammak, A. et al. Shallow and undoped Germanium quantum wells: a playground for spin and hybrid quantum technology. *Adv. Funct. Mater.* **29**, 1807613 (2019).
13. Studenikin, S. et al. Electrically tunable effective g-factor of a single hole in a lateral GaAs/AlGaAs quantum dot. *Commun. Phys.* **2**, 159 (2019).
14. Croke, E. T. et al. Direct electrical measurement of the electron g factor in ultra-thin InGaAs/InP single quantum wells. *Microelectron. J.* **36**, 379–382 (2005).
15. Dobers, M., Vonklitzing, K. & Weimann, G. Electron-spin resonance in the two-dimensional electron-gas of GaAs-AlGaAs heterostructures. *Phys. Rev. B* **38**, 5453–5456 (1988).
16. Salis, G. et al. Electrical control of spin coherence in semiconductor nanostructures. *Nature* **414**, 619–622 (2001).
17. Pioro-Ladriére, M. et al. Electrically driven single-electron spin resonance in a slanting Zeeman field. *Nat. Phys.* **4**, 776–779 (2008).
18. Ito, T. et al. Four single-spin Rabi oscillations in a quadruple quantum dot. *Appl. Phys. Lett.* **113**, 093102 (2018).
19. Forster, F., Mühlbacher, M., Schuh, D., Wegscheider, W. & Ludwig, S. Electric-dipole-induced spin resonance in a lateral double quantum dot incorporating two single-domain nanomagnets. *Phys. Rev. B* **91**, 195417 (2015).
20. Gilbert, W. et al. On-demand electrical control of spin qubits. *Nat. Nanotechnol.* https://doi.org/10.1038/s41565-022-01280-4 (2023)
21. Zajac, D. M., Hazard, T. M., Mi, X., Nielsen, E. & Petta, J. R. Scalable gate architecture for a one-dimensional array of semiconductor spin qubits. *Phys. Rev. Appl.* **6**, 054013 (2016).
22. Veldhorst, M. et al. An addressable quantum dot qubit with fault-tolerant control-fidelity. *Nat Nano* **9**, 981–985 (2014). http://www.nature.com/nnano/journal/v9/n12/abs/nnano.2014.216.html#supplementary-information
23. Liles, S. D. et al. Electrical control of the g tensor of the first hole in a silicon MOS quantum dot. *Phys. Rev. B* **104**, 235303 (2021).
24. Crippa, A. et al. Electrical spin driving by g-Matrix modulation in spin-orbit Qubits. *Phys. Rev. Lett.* **120**, 137702 (2018).
25. Winkler, R. *Spin-Orbit Coupling Effects in Two-Dimensional Electron and Hole Systems, Springer Tracts in Modern Physics*. (Springer Berlin, 2003).
26. Studenikin, S. et al. Single-hole physics in GaAs/AlGaAs double quantum dot system with strong spin-orbit interaction. *Semicond. Sci. Technol.* **36**, 053001 (2021).

27. Teske, J. D. et al. A machine learning approach for automated fine-tuning of semiconductor spin qubits. *Appl. Phys. Lett.* **114**, 133102 (2019).
28. Terrazos, L. A. et al. Theory of hole-spin qubits in strained germanium quantum dots. *Phys. Rev. B* **103**, 125201 (2021).
29. Marton, V., Sachrajda, A., Korkusinski, M., Bogan, A. & Studenikin, S. Coherence characteristics of a GaAs single heavy-hole spin Qubit using a modified single-shot latching readout technique. *Nanomaterials* **13**, 950 https://www.mdpi.com/2079-4991/13/5/950 (2023).
30. Bogan, A. et al. Consequences of spin-orbit coupling at the single hole level: spin-flip tunneling and the anisotropic g factor. *Phys. Rev. Lett.* **118**, 167701–167705 (2017).
31. Morrison, C. & Myronov, M. Strained germanium for applications in spintronics. *Phys. Status Solidi (a)* **213**, 2809–2819 (2016).
32. Bogan, A. et al. Single hole spin relaxation probed by fast single-shot latched charge sensing. *Commun. Phys.* **2**, 17 (2019).
33. von Klitzing, K. et al. 40 years of the quantum Hall effect. *Nat. Rev. Phys.* **2**, 397–401 (2020).
34. Nedniyom, B. et al. Giant enhanced g-factors in an InSb two-dimensional gas. *Phys. Rev. B* **80**, 125328 (2009).
35. Brosig, S. et al. InAs-AlSb quantum wells in tilted magnetic fields. *Phys. Rev. B* **61**, 13045 (2000).
36. Isihara, A. & Smrcka, L. Density and magnetic field dependences of the conductivity of two-dimensional electron systems. *J. Phys. C: Solid State Phys.* **19**, 6777 (1986).
37. Coleridge, P. T., Hayne, M., Zawadzki, P. & Sachrajda, A. S. Effective masses in high-mobility 2D electron gas structures. *Surf. Sci.* **361-362**, 560–563 (1996).
38. Piot, B. A. et al. Quantum Hall ferromagnet at high filling factors: A magnetic-field-induced Stoner transition. *Phys. Rev. B* **72**, 245325 (2005).
39. Morrison, C. & Myronov, M. Electronic transport anisotropy of 2D carriers in biaxial compressive strained germanium. *Appl. Phys. Lett.* **111**, 192103 (2017).
40. Tan, Y. W. et al. Measurements of the density-dependent many-body electron mass in two dimensional GaAs/AlGaAs heterostructures. *Phys. Rev. Lett.* **94**, 016405 (2005).
41. Lodari, M. et al. Light effective hole mass in undoped Ge/SiGe quantum wells. *Phys. Rev. B* **100**, 041304 (2019).
42. Mi, X. et al. Magnetotransport studies of mobility limiting mechanisms in undoped Si/SiGe heterostructures. *Phys. Rev. B* **92**, 035304 (2015).
43. Yang, C. H. et al. Operation of a silicon quantum processor unit cell above one kelvin. *Nature* **580**, 350–354 (2020).
44. Camenzind, L. C. et al. A hole spin qubit in a fin field-effect transistor above 4 kelvin. *Nat. Electron.* **5**, 178–183 (2022).
45. Maurand, R. et al. A CMOS silicon spin qubit. *Nat. Commun.* **7**, 13575 (2016).
46. Wang, C.-A., Scappucci, G., Veldhorst, M. & Russ, M. in arXiv: [cond-mat.mes-hall] https://arxiv.org/abs/2208.04795 (2022).
47. Lu, T. M. et al. Effective g factor of low-density two-dimensional holes in a Ge quantum well. *Appl. Phys. Lett.* **111**, 102108 (2017).
48. Koppens, F. H. L. et al. Driven coherent oscillations of a single electron spin in a quantum dot. *Nature* **442**, 766–771 (2006).
49. Vahapoglu, E. et al. Single-electron spin resonance in a nanoelectronic device using a global field. *Sci. Adv.* **7**, eabg9158 (2021).
50. Mizokuchi, R., Maurand, R., Vigneau, F., Myronov, M. & De Franceschi, S. Ballistic one-dimensional holes with strong g-Factor Anisotropy in Germanium. *Nano Lett.* **18**, 4861–4865 (2018).
51. Coleridge, P. T., Stoner, R. & Fletcher, R. Low-field transport coefficients in GaAs/Ga_{1-x}Al_{x}As heterostructures. *Phys. Rev. B* **39**, 1120 (1989).
52. Coleridge, P. T. Small-angle scattering in two-dimensional electron gases. *Phys. Rev. B* **44**, 3793 (1991).
53. Xie, X. C., Li, Q. P. & Das Sarma, S. Density of states and thermodynamic properties of a two-dimensional electron gas in a strong external magnetic field. *Phys. Rev. B* **42**, 7132–7147 (1990).
54. Dial, O. E., Ashoori, R. C., Pfeiffer, L. N. & West, K. W. Anomalous structure in the single particle spectrum of the fractional quantum Hall effect. *Nature* **464**, 566–570 (2010).
55. Krishtopenko, S. S. et al. Exchange enhancement of the electron g factor in strained InGaAs/InP heterostructures. *Semiconductors* **49**, 191–198 (2015).
56. Ando, T., Fowler, A. B. & Stern, F. Electronic properties of two-dimensional systems. *Rev. Mod. Phys.* **54**, 437–672 (1982).
57. Fogler, M. M. & Shklovskii, B. I. Collapse of spin splitting in the quantum Hall effect. *Phys. Rev. B* **52**, 17366–17378 (1995).
58. Leadley, D. R., Nicholas, R. J., Harris, J. J. & Foxon, C. T. Critical collapse of the exchange-enhanced spin splitting in two-dimensional systems. *Phys. Rev. B* **58**, 13036 (1998).
59. Pan, W., Baldwin, K. W., West, K. W., Pfeiffer, L. N. & Tsui, D. C. Quantitative examination of the collapse of spin splitting in the quantum Hall regime. *Phys. Rev. B* **84**, 161307 (2011).
60. Kernreiter, T., Governale, M., Winkler, R. & Zülicke, U. Suppression of Coulomb exchange energy in quasi-two-dimensional hole systems. *Phys. Rev. B* **88**, 125309 (2013).

Acknowledgements

We thank Dr Alan Burton for technical support of equipment and clean room facilities at Warwick.The Authors thank the financial support of the National Research Council's Quantum Sensors Challenge Program.

Author contributions

M.M. and S.S. designed the experiment and wrote the article, M.M. developed the CVD growth technology and prepared the s-Ge epi wafers, MM, S.S., P.W. and P.B. developed the fabrication technology and P.W. and P.B. fabricated the gated Hall bar device, A.B. provided with the data acquisition programming and the experiment automatization, S.S. conducted the low temperature measurements and analysed the magneto-transport data.

Competing interests

The authors declare no competing interests.

Additional information

Supplementary information The online version contains supplementary material available at https://doi.org/10.1038/s43246-023-00431-x.

Correspondence and requests for materials should be addressed to Maksym Myronov or Sergei Studenikin.

Peer review information *Communications Materials* thanks the anonymous reviewers for their contribution to the peer review of this work. Primary Handling Editor: Aldo Isidori. A peer review file is available.

Reprints and permission information is available at http://www.nature.com/reprints

Publisher's note Springer Nature remains neutral with regard to jurisdictional claims in published maps and institutional affiliations.

Open Access This article is licensed under a Creative Commons Attribution 4.0 International License, which permits use, sharing, adaptation, distribution and reproduction in any medium or format, as long as you give appropriate credit to the original author(s) and the source, provide a link to the Creative Commons licence, and indicate if changes were made. The images or other third party material in this article are included in the article's Creative Commons licence, unless indicated otherwise in a credit line to the material. If material is not included in the article's Creative Commons licence and your intended use is not permitted by statutory regulation or exceeds the permitted use, you will need to obtain permission directly from the copyright holder. To view a copy of this licence, visit http://creativecommons.org/licenses/by/4.0/.

© The Author(s) 2023